



**HAL**  
open science

## Dry granular flows: Rheological measurements of the $\mu(I)$ -rheology

Abdoulaye Fall, Guillaume Ovarlez, David Hautemayou, Cédric Mézière,  
Jean-Noël Roux, François Chevoir

### ► To cite this version:

Abdoulaye Fall, Guillaume Ovarlez, David Hautemayou, Cédric Mézière, Jean-Noël Roux, et al.. Dry granular flows: Rheological measurements of the  $\mu(I)$  -rheology. *Journal of Rheology*, 2015, 59 (4), pp.1065. 10.1122/1.4922653 . hal-01165682

**HAL Id: hal-01165682**

**<https://enpc.hal.science/hal-01165682v1>**

Submitted on 27 Jun 2019

**HAL** is a multi-disciplinary open access archive for the deposit and dissemination of scientific research documents, whether they are published or not. The documents may come from teaching and research institutions in France or abroad, or from public or private research centers.

L'archive ouverte pluridisciplinaire **HAL**, est destinée au dépôt et à la diffusion de documents scientifiques de niveau recherche, publiés ou non, émanant des établissements d'enseignement et de recherche français ou étrangers, des laboratoires publics ou privés.

# Dry granular flows: rheological measurements of the $\mu(I)$ -rheology

A. Fall<sup>1</sup>, G. Ovarlez<sup>1,2</sup>, D. Hautemayou<sup>1</sup>, C. Mézière<sup>1</sup>, J.-N. Roux<sup>1</sup> and F. Chevoir<sup>1</sup>

<sup>1</sup> *Université Paris Est, Laboratoire Navier (CNRS, IFSTTAR, Ecole des Ponts ParisTech),  
Champs-sur-Marne, France*

<sup>2</sup> *CNRS, LOF, UMR 5258, F-33600 Pessac, France*

Dated 01 June 2015

## Synopsis

Granular materials do not always flow homogeneously like fluids when submitted to external stress, but often form rigid regions that are separated by narrow shear bands where the material yields and flows. This shear localization impacts their apparent rheology, which makes it difficult to infer a constitutive behaviour from conventional rheometric measurements. Moreover, they present a dilatant behaviour, which makes their study in classical fixed-volume geometries difficult. These features led numerous groups to perform extensive studies with inclined plane flows, which were of crucial importance for the development and the validation of the  $\mu(I)$ -rheology. Our aim is to develop a method to characterize granular materials with rheometrical tools. Using rheometry measurements in an annular shear cell, dense granular flows of 0.5 mm spherical and monodisperse beads are studied. A focus is placed on the comparison between the present results and the  $\mu(I)$ -rheology. From steady state measurements of the torque and the gap under imposed shear rate  $\dot{\gamma}$  and normal force  $F_N$ , we define an inertial number  $I$ . We show that, at low  $I$  (small  $\dot{\gamma}$  and/or large  $F_N$ ), the flow goes to a quasi-static limit, and the response in terms of dimensionless stress or internal friction coefficient  $-\mu$  – and solid concentration  $-\phi$  – profiles is independent of the inertial number. Upon increasing  $I$  (large  $\dot{\gamma}$  and/or small  $F_N$ ), dilation occurs and  $\phi$  decreases while  $\mu$  increases. The observed variations are in good agreement with previous observations of the literature (Jop et al. 2006; Hatano 2007). These results show that the constitutive equations  $\mu(I)$  and  $\phi(I)$  of granular materials can be measured with a rheometer.

## 32 **I. Introduction**

33 Granular matter shows both solid and fluid behavior. Of interest in many industrial processes  
34 and in geophysics, granular flows are the focus of very active researches (Duran 2000). These  
35 materials are very sensitive to various parameters: geometry of the flow, wall roughness, flow  
36 rate, shape and size distribution of the grains, and coupling with the interstitial fluid  
37 (Andreotti et al. 2013). Due to their macroscopic size, the interactions between the grains are  
38 dissipative (friction and inelastic collisions); the energy lost is then transferred to internal  
39 degrees of freedom. The lack of Brownian motion and the dissipative interactions, make the  
40 granular material an intrinsically nonequilibrium system.

41 In the dry case – *without interstitial fluid* –, the rheology is solely governed by momentum  
42 transfer and energy dissipation occurring in direct contacts between grains and with the walls.  
43 Despite the seeming simplicity of the system, the behavior of dry granular material is very  
44 rich and extends from solid to gaseous properties depending on the flow regime. In the  
45 absence of a unified framework, granular flows are generally divided into three different  
46 regimes. (i) At low shear, particles stay in contact and interact frictionally with their  
47 neighbours over long periods of time. This “quasi-static” regime of granular flow has been  
48 classically studied using modified plasticity models based on a Coulomb friction criterion  
49 (Schofield & Wroth 1968; Becker and Lippmann 1977). The response in terms of velocity or  
50 solid fraction profiles is independent of the shear rate (Roux & Combe 2002; GDR Midi  
51 2004). Consequently, if the material remains homogeneous, this state only depends on  
52 geometric data (shape and size distribution of the grains) and on the inter-granular friction  
53 coefficient. (ii) Upon increasing the deformation rate, a viscous-like regime occurs and the  
54 material flows more as a liquid (Forterre & Pouliquen 2008). In this intermediate regime, the  
55 particles experience multi-contact interactions. (iii) At very high velocity, a transition occurs  
56 towards a gaseous regime, in which the particles interact through binary collisions  
57 (Goldhirsch 2003; Jenkins and Savage 1983).

58 For the modelling of dense granular flows, the concept of inertial number  $I$  has been widely  
59 used and investigated with regard to its relationship with dynamic parameters, such as  
60 velocity, stress, and friction coefficient which leads to constitutive relations for granular  
61 flows. Thus, ‘*dynamic dilatancy*’ law and ‘*friction*’ law were deduced from discrete  
62 simulation of two dimensional simple shear of a granular material without gravity (da Cruz et  
63 al. 2005). Those results establish that the flow regime and rheological parameters depend on a  
64 single dimensionless number that represents the relative strength of inertia forces with respect

65 to the confining pressure, or the combined effect of pressure and shear rate. Indeed, for a  
66 three-dimensional granular medium made up of monodisperse spheres ( $d, \rho$  resp. the  
67 particle's diameter and density) undergoing simple shear flow at a shear rate  $\dot{\gamma}$  under an  
68 applied normal confining stress  $\sigma$ , this dimensionless number – inertial number – is defined  
69 as  $I = \dot{\gamma}d / \sqrt{\sigma / \rho}$ . Alternatively, one may use the Savage number which is the square of the  
70 inertial number (Savage & Hutter 1989) or the Coulomb number (Ancy et al. 1999, see also  
71 GDR Midi 2004; Baran & Kondic 2006; Hatano 2007; Luding 2008). Dimensionless number  
72  $I$  can also be seen as the ratio of  $d / \sqrt{\sigma / \rho}$ , the time scale for grains to rearrange due to the  
73 confining stress  $\sigma$ , to the time scale  $\dot{\gamma}^{-1}$  for deformation by the flow. Hence, it characterizes  
74 the local ‘‘rapidity’’ of the flow. Thus it was observed that both dimensionless quantities: the  
75 internal friction coefficient  $\mu = \tau / \sigma$  and the solid fraction  $\phi$  are functions of  $I$  (GDR Midi  
76 2004; da Cruz et al. 2005; Hatano 2007). Thereby, the inertial number  $I$  opened a new path  
77 unifying, in a single phenomenological law, many experimental and numerical data in a wide  
78 variety of transient flows from the rotating drum to inclined plane flows, where large flowing  
79 zones form. A local relation between an apparent friction coefficient and  $I$  then successfully  
80 captures many aspects of these rapid granular flows (Savage & Hutter 1989; GDR Midi 2004;  
81 Jop et al. 2006; Forterre & Pouliquen 2008).

82 Following general results from simulations of planar shear (da Cruz et al. 2005; Iordanoff &  
83 Khonsari 2004), and successful applications to inclined plane flows (Pouliquen & Forterre  
84 2002; Silbert et al. 2003), the experiments of Jop and co-workers (Jop et al. 2006) were  
85 carried out to quantify, for glass beads, the  $\mu(I)$ –rheology from the quasi-static to the rapid  
86 flow regime, corresponding to moderate inertial number (from 0.01 to 0.5) as:

$$87 \quad \mu = \mu_s + (\mu_2 - \mu_s) / (1 + I_0 / I) \quad (1)$$

88 in which  $\mu_s, \mu_2$  and  $I_0$  are three fitting parameters dependent on material properties.  
89 According to this law, the internal friction coefficient  $\mu$  goes from a minimum value  $\mu_s$  for  
90 very low  $I$  up to an asymptotic value  $\mu_2$  when  $I$  increases. The asymptotic value of  $\mu$  at  
91 high inertial number was not obtained by da Cruz and co-workers who observed an  
92 approximately linear increase of the internal friction coefficient from the static internal  
93 friction value:

$$94 \quad \mu = \mu_s + aI \quad (2)$$

95 where  $\mu_s$  and  $a$  are two fitting parameters which depend on material properties. In 3D-  
 96 simulation studies, Hatano did not either observe the asymptotic value of  $\mu$  at high  $I$ : from  
 97  $I = 10^{-4}$  to  $I = 0.2$ , he reported a law in which the friction coefficient increases as a power of  
 98 the inertial number (Hatano 2007):

$$99 \quad \mu = \mu_s + aI^n \quad (3)$$

100 It should be pointed out however that this rheology agrees with earlier scaling relations  
 101 stemming back to Bagnold (Bagnold 1954). Bagnold described a mechanism of momentum  
 102 transfer between particles in adjacent layers that assumes instantaneous binary collisions  
 103 between the particles during the flow. Under this assumption, the inverse strain rate is the  
 104 only relevant time scale in the problem leading, for a constant solid fraction  $\phi$ , to constitutive  
 105 relations between the shear stress  $\tau$  (resp. normal stress  $\sigma$ ) and shear rate  $\dot{\gamma}$  of the form  
 106  $\tau = \rho d^2 f_1(\phi) \dot{\gamma}^2$  (resp.  $\sigma = \rho d^2 f_2(\phi) \dot{\gamma}^2$ ) where  $f_1$  and  $f_2$  are functions of the solid fraction  $\phi$   
 107 only. Bagnold's scaling has been verified for dry grains in both collisional and dense flow  
 108 regimes (Jenkins & Savage 1983; Lois et al. 1987; Silbert et al. 2001; Lois et al. 2005; da  
 109 Cruz et al. 2005). The main difference between the *Bagnold* and  $\mu(I)$  approaches is that: in  
 110 the first case,  $\phi$  is kept constant for one given flow, whereas it varies freely and depends on  
 111 the flow in the second case. Indeed, if the pressure is controlled, the solid fraction  $\phi$  is free to  
 112 adapt in the system with the evolution of other parameters. If  $\phi$  is fixed however and the  
 113 normal pressure measured, this will fix the value of  $I$ . Then when  $\phi$  is fixed, the expression  
 114 of  $I$  shows that the normal pressure should scale with the square of the shear rate as it was  
 115 shown experimentally in annular parallel-plate shear cell (Savage & Sayed 1984).

116

117 The applicability of the  $\mu(I)$ -rheology has been examined by various studies (Jop et al.  
 118 2005, 2006; Hatano 2007; Forterre & Pouliquen 2008; Ruck et al. 2008; Aranson et al. 2008;  
 119 Peyneau & Roux 2008; Staron et al. 2010; Gaume et al. 2011; Tripathi & Khakhar 2011;  
 120 Chialvo et al. 2012; Azéma & Radjai, 2014; Gray & Edwards 2014; Edwards & Gray 2015)  
 121 and many simulations and experiments have shown that the rheology is valid for various flow  
 122 configurations for different choices of materials, although deviations from this rheology may  
 123 take place for very slow (quasi-static) flows with small values of inertial number (Aranson et  
 124 al. 2008; Staron et al. 2010; Gaume et al. 2011). Up to now, there is however in the literature,  
 125 no experimental data from conventional rheology (*rheometer with conventional geometries*)  
 126 describing the  $\mu(I)$ -rheology of a dry granular material. Indeed, *Couette flows* of granular

127 materials are characterized by the formation of well-defined shear bands that resemble  
128 qualitatively the behavior of a yield stress fluid, and make the interpretation of rheometric  
129 data tricky. For slow flows, shear banding is generally very strong, with shear bands having a  
130 typical thickness of five to ten grain diameters. In this regime of slow flow, the averaged  
131 stresses and flow profiles become essentially independent of the flow rate, so that constitutive  
132 relations based on relating stresses and strain rates are unlikely to capture the full physics  
133 (Schofield & Wroth 1968; Nedderman 1992; Fenistein & van Hecke 2003; Fenistein et al.  
134 2004). Moreover, due to the dilatant behaviour of granular materials, *constant solid fraction*  
135  $\phi$  experiments classically made with a Couette shear-cell rheometer are much more difficult  
136 to perform than *constant friction coefficient*  $\mu$  experiments such as inclined plane flows.  
137 When a granular matter is sheared, the spatial distribution of the shear rate is not always  
138 homogeneous. Often, shear is localized near the system boundaries with a shear localization  
139 width amounting to a few particle diameters. Nevertheless, depending on the boundary  
140 conditions, confining pressure and shear velocity, the bulk of the granular system may exhibit  
141 different behaviours. For high shear velocities and small confining pressures – *high  $I$*  –, the  
142 granular matter flows homogeneously (Koval et al. 2009). However, at small inertial number,  
143 it was indeed shown that in confined annular flow at small shear velocities and high confining  
144 pressures – *small  $I$*  –, the shear may be not homogeneous and solid and fluid phases coexist  
145 (Aharonov & Sparks 2002; Jalali et al. 2002).

146

147 In the present work, we show that it is not necessary to develop specific set-ups (such as the  
148 inclined plane) to study dense granular flows. Indeed, we show that a simple annular shear  
149 cell (Carr and Walker 1968, Savage and Sayed 1984) can be adapted to a standard rheometer  
150 to study the rheology of granular materials under controlled confining pressure. It allows us in  
151 particular to obtain the dilatancy law  $\phi(I)$  and also to study very accurately the quasi-static  
152 limit. Thus, from the steady state measurements of the torque and the gap during an imposed  
153 shear flow under an applied normal confining stress  $\sigma$ , we report two laws in which the  
154 internal friction coefficient and the solid fraction are functions of a single dimensionless  
155 number: the inertial number  $I$ . An effort is then made to compare the present results to the  
156  $\mu(I)$ -rheology described in the literature. Indeed, we show that at low inertial number  $I$   
157 (small  $\dot{\gamma}$  and/or large  $\sigma$ ), the flow goes to the quasi-static limit, and the response in terms of  
158 internal friction coefficient  $\mu$  and solid fraction  $\phi$  profiles is independent of the inertial  
159 number. Upon increasing  $I$  (large  $\dot{\gamma}$  and/or small  $\sigma$ ),  $\phi$  decreases while  $\mu$  increases. The

160 observed variations are in good agreement with previous observations of the literature.  
161 Importantly, we also show that changing the initial gap size does not significantly affect these  
162 results. This suggests that shear localization is mostly absent in the intermediate dense flow  
163 regime, although it may still occur when the granular material is slowly sheared (in the quasi-  
164 static regime).

165

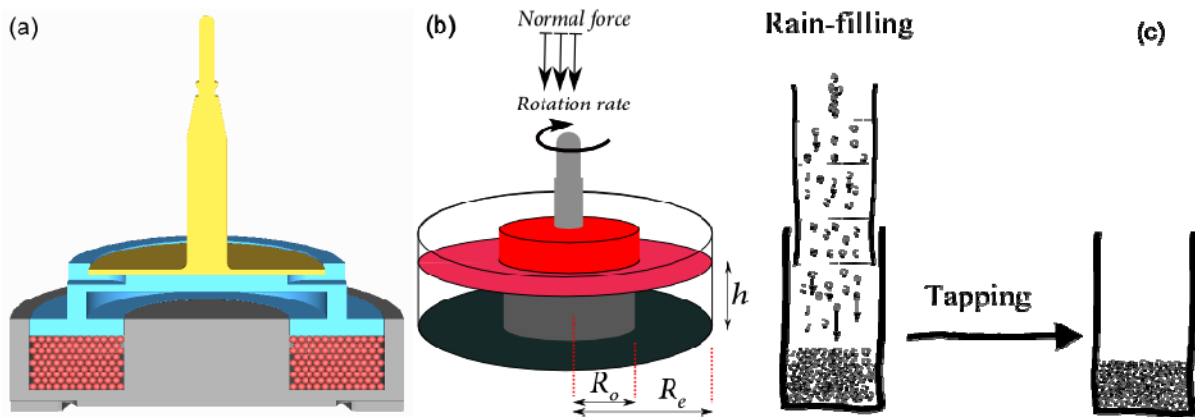
## 166 **II. Materials and methods**

167 To investigate the steady flows of dry granular materials and determine the  $\mu(I)$ -rheology,  
168 three main features are required: (i) to avoid shear banding, (ii) to apply a confining stress in  
169 the velocity gradient direction, and (iii) to allow volume fraction variations. If one wants to  
170 use a rheometer, (i) implies that the use of a Couette cell should be avoided since it is  
171 characterized by a shear stress inhomogeneity that naturally leads to shear-banding. Both the  
172 cone-and-plate and the parallel-plate geometries allow a normal force to be imposed in the  
173 velocity gradient direction; however, the analysis of the cone-and-plate flow can be performed  
174 only at a single gap value, i.e. it cannot be used to characterize a material whose the volume  
175 varies under shear. On the other hand, any gap variation in parallel-plate geometry can be  
176 accounted for in the determination of the shear rate value. Moreover, shear banding should in  
177 principle be avoided in this last geometry since the shear stress is independent of the vertical  
178 position in the gap (Macosko 1993). Nevertheless, the shear rate varies along the radial  
179 position and is equal to zero in the center. One should thus try to avoid the use of the central  
180 zone of the gap. Finally, the material should be confined by lateral walls to make sure that any  
181 gap variation actually leads to a material volume fraction variation. These requirements led us  
182 to develop a home made annular shear cell, inspired by Boyer et al. 2011, in which pressure-  
183 imposed measurements can be performed as shown in Figure 1. Annular shear cells have been  
184 extensively used to characterize the flow of pharmaceutical powders and dry granular  
185 materials (Carr and Walker 1968, Savage and Sayed 1984, Schulze 1996; Schwedes 2003).

186 We use a granular material made of rigid polystyrene beads (from Dynoseeds) of density  
187  $\rho = 1050 \text{ kg/m}^3$ , of diameter  $d = 0.5 \text{ mm}$  (with a standard deviation of 5%). Spherical beads  
188 fill the annular box between two static concentric cylinders with respectively an inner and  
189 outer radii of  $R_i = 21 \text{ mm}$  and  $R_o = 45 \text{ mm}$ . The width of the annular trough is about  $48d$   
190 leading to a ratio of inner to outer wall radii of 0.46. We also used another annular channel  
191 with the same width but with a larger ratio of inner to outer cylinder radii equal to 0.61  
192 ( $R_i = 38 \text{ mm}$  and  $R_o = 62 \text{ mm}$ ). We have verified that changing the ratio of inner to outer

193 cylinder radii of the annular shear cell does not significantly affect the results. The filling  
 194 height (initial gap,  $h_0$ ) of the annular box is adjustable from a few grain diameters (typically  
 195  $5d$ ) to  $30d$ . The cylinders were finished as smoothly as possible to permit the granular  
 196 material to slip there as readily as possible. For that, they are made of polyoxymethylene  
 197 (POM) resin which exhibits a low friction coefficient due to the flexibility of the linear  
 198 molecular chains. We have measured the friction coefficient at the wall  $\mu_w$  between  
 199 polystyrene beads and a plane made of POM by measuring with our rheometer the sliding  
 200 stress under different normal stresses such as in Jenike's shear tester (Jenike 1964; Schwedes  
 201 2003); it is found to be very small:  $\mu_w \approx 0.05$ .

202



203

204

205 Figure 1: (a-b) Cross section of the annular plane shear flow. The shear and pressure are  
 206 provided by a ring which is assembled on a *Kinexus* rheometer by *Malvern* that is free to  
 207 move vertically while maintaining a constant rotation rate or shear rate and imposed pressure.  
 208 (c) Rain-filling coupled to tapping to get the denser piling sample ('D').

209

210 The experiments were performed initially on a very dense piling  $\phi_0 \approx 0.625$ , close to the so  
 211 called random close packing of 0.637 (Torquato et al. 2000; Camenen et al. 2012) obtained by  
 212 combining a rain-filling and tapping the box (Ovarlez et al. 2003) to get a reasonably uniform  
 213 packing (Figure 1b). However, we will show below that the steady state obtained when the  
 214 material is sheared is the same for an initially looser piling (Figure 2c). Granular beads are  
 215 then driven by the ring-shaped upper boundary made of PMMA, which is assembled on a  
 216 *Kinexus Pro* rheometer by *Malvern*. To avoid wall slip, both the moving upper boundary and  
 217 the static lower boundary are serrated, with  $0.5 \text{ mm}$  ridges which correspond to the size of  
 218 grains (Shojaee et al. 2012).



219

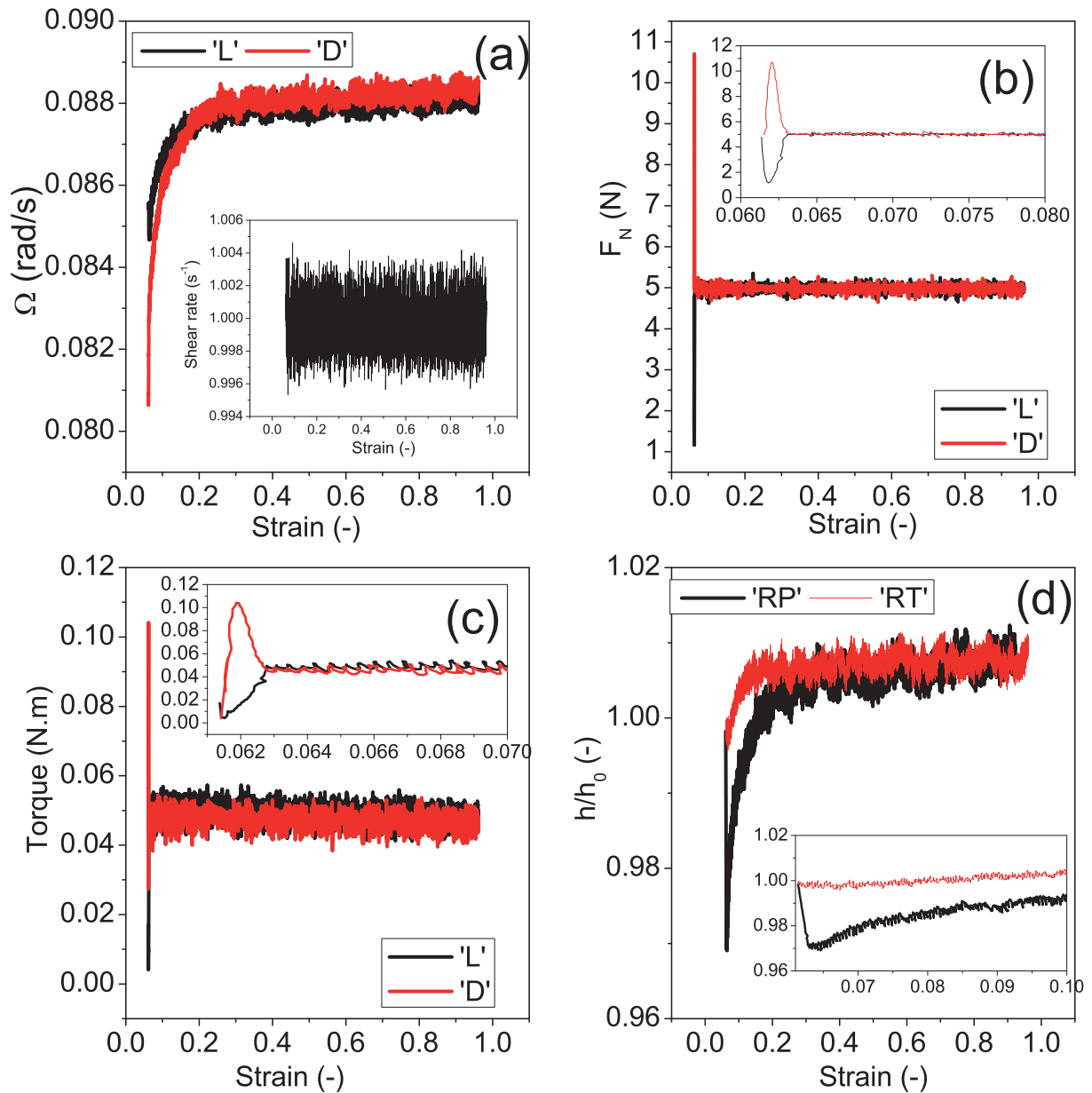
220 In our rheometer, instead of setting the value of the gap size for a given experiment, as in  
221 previous studies (Schulze 1996; Schwedes 2003) and generally in rheometric measurements,  
222 we impose the normal force (i.e. the confining normal stress) and then, under shear, we let the  
223 gap size vary in order to maintain the desired value of the normal force. We then have access  
224 to instantaneous measurements of the driving torque  $T$  and the gap  $h$  for imposed normal  
225 force  $F_N$  and shear rate  $\dot{\gamma}$ : in this case, the solid fraction  $\phi$  is not fixed, but adjusts to the  
226 imposed shear. However, it remains important to notice that, in order to keep the imposed  
227 shear rate constant, the rheometer adjusts the rotation velocity  $\Omega$  since the gap varies as will  
228 be discussed below.

229

230 A typical measurement is shown in Figure 2, where we start out with a given gap  $h_0 \approx 6d$ ,  
231 impose a constant shear rate  $\dot{\gamma}$  and normal force  $F_N$  and measure the torque  $T$  and the gap  
232  $h$  as a function of strain (or time). The system reaches a steady state after a certain amount of  
233 shear strain but we carefully compare the transient dynamics of these quantities, beginning  
234 with freshly poured grains for two preparations, ‘rain piling’ and ‘rain coupled to tapping  
235 piling’ (resp.) which allow us to get the looser (‘L’) piling and the denser (‘D’) piling (resp.)  
236 samples with an initial solid fraction of 0.612 and 0.625 (resp.).

237 Let us start with the imposed quantities. In both cases, a small variation of the rotation  
238 velocity is seen (Figure 2a). As discussed above, this variation is a signature of the shear-  
239 induced gap variations; it ensures that the shear rate is constant at any time or strain (see  
240 inset). We also see that, in both cases, the normal force reaches quickly the stationary targeted  
241 value and remains steady during the whole experiment (Figure 2b). Nevertheless, the short  
242 transient behavior is different: in the looser sample (‘L’), a significant decrease of the normal  
243 force is initially observed while a very sharp increase is observed in the densest piling (‘D’).  
244 The reason is that the densest system initially wants to dilate, and the rheometer response is  
245 not fast enough to allow for this fast dilation at constant normal force. By contrast, the loose  
246 sample initially wants to compact, and again the rheometer response is not fast enough to  
247 allow for this fast compaction at constant normal force.

248



249

250 Figure 2: Comparison between samples from the two different pilings: rain piling (which  
 251 allows us to get the looser piling sample 'L') and rain piling coupled to tapping (that lets us to  
 252 get the denser piling sample 'D') of the (a) rotational rate against strain; Inset: the imposed  
 253 shear rate vs. strain, (b) imposed normal force as a function of strain, (c) driving torque and  
 254 (d) gap size rescaled by the initial gap against strain. The insets in (b-c-d) are the same data  
 255 showing the sharp increase/decrease of the normal force, the overshoot of the torque and the  
 256 gap change at the beginning of shearing.

257

258 The transient dynamics of the measured quantities (torque and gap size) also shows a clear  
 259 difference between the two samples. In Figure 2c, we see that, in the loosest piling ('L'), the  
 260 torque increases before reaching the steady state regime. By contrast, there is an overshoot

261 within the densest sample ('D'), followed by a fast decrease of the torque: the peak strongly  
262 depends on the imposed normal force and/or on the shear rate; the decrease corresponds to the  
263 continuous dilation of the material under shear. Indeed, in the same time, the gap is not fixed,  
264 but adjusts to the imposed shear (Figure 2d). Shear dilation is observed: the measured gap  
265 increases up to a constant value since the average of the initial solid fraction is very close to  
266 the random close packing. In this regime, shearing necessarily implies immediate dilatancy of  
267 the granular media. In contrast, an initially looser sample first compact instead of dilate under  
268 shear: when the system is driven under a fixed normal pressure, the granular packing  
269 undergoes compaction before dilation into the final state once sufficiently compacted (Wroth  
270 1958).

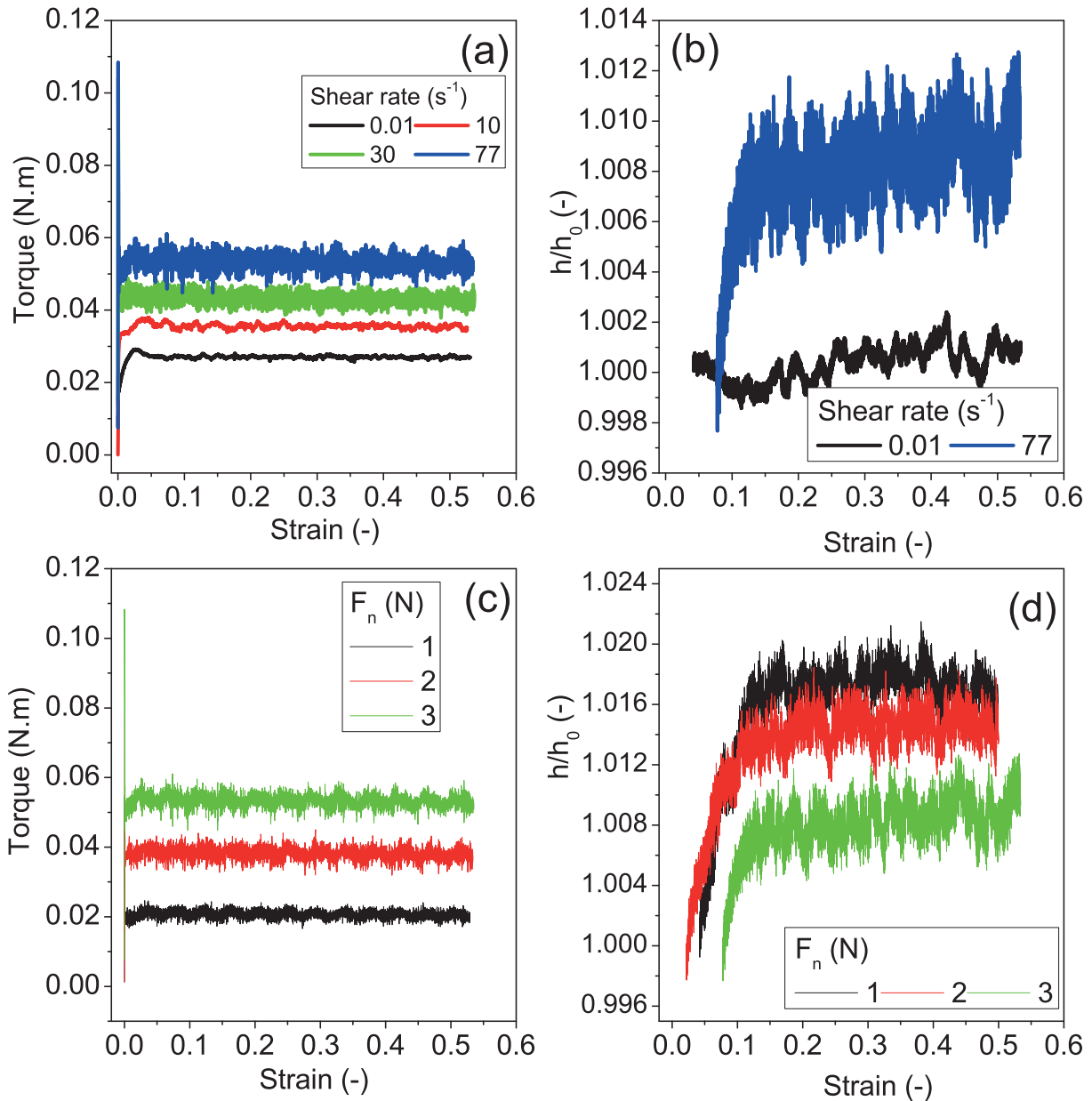
271  
272 The most important observation is that the same steady state is reached (same torque and  
273 same solid fraction) for the two initial states. This indicates that the material history has been  
274 erased, and that we are actually studying the material steady response as a function of  $\dot{\gamma}$  and  
275  $F_N$  only. As a consequence, there is no need for the sample preparation for the grains we  
276 study, namely monodisperse spheres (note that this might not be a general result). All the  
277 annular shear cell requires is that the sample is sheared at the required normal pressure until  
278 the critical state is reached. However it is necessary to adopt a reference packing state and  
279 ensure that the piling method used allows us to achieve sufficient repeatability for a given set  
280 materials and system parameters. Hence, we prepare all samples in the same way: a very  
281 dense material, from a rain piling coupled to tapping, is used in all the experiments presented  
282 below (the initial average volume fraction is 0.625).

283

### 284 **III. Experimental results and analyses**

285 We have measured the driving torque and the gap as a function of shear strain for various  
286 imposed normal force  $F_N$  (between 1 and 5N) and applied shear rate  $\dot{\gamma}$  (between 0.01  
287 and 77 s<sup>-1</sup>) for a given gap  $h_0 \approx 6d$ .

288 In Figure 3 (a, b), we show those measurements for  $F_N = 3N$  and various  $\dot{\gamma}$ . At low shear  
289 rate, the driving torque increases slowly before reaching a steady plateau within strain of  
290 order of unity. Meanwhile, the gap fluctuates around its initial value (we show the gap size  
291 rescaled by its initial value before shearing  $h/h_0$  called the rescaled gap in the following.).



292

293 Figure 3: Evolution as a function of the strain at 3N imposed normal force under different  
 294 applied shear rates of: (a) the driving torque and (b) the rescaled gap size (only 2 curves are  
 295 shown for clarity). Evolution as a function of the strain at 77 s<sup>-1</sup> imposed shear rate under  
 296 different applied normal forces of: (c) the driving torque and (d) the gap size rescaled by its  
 297 initial value before shearing.

298

299 Upon increasing the imposed shear rate, an overshoot occurs: its amplitude increases with  
 300 increasing the shear rate. In steady state, a rate dependence of the torque is observed (Figure  
 301 3a). Moreover, increasing the imposed shear rate causes an increase of the gap size (Figure  
 302 3b) allowing to quantify the dynamic dilatancy of the granular material. Notice that, with

303 increasing the applied shear rate, large fluctuations of the driving torque and also of the gap  
304 size evolution occur in steady state flows.

305 Similarly, in experiments in which different normal forces are imposed at a given shear rate  
306 (Figure 3c, d), the steady torque is observed to increase while the steady solid fraction (steady  
307 gap) decreases when the normal force is increased.

308 Once the above described experiments are combined, we can obtain the constitutive laws of  
309 the dry granular material i.e. the dependence of the steady solid fraction  $\phi$  and the ratio  
310 between shear and normal stresses  $\tau/\sigma$  variation on shear rate. Indeed, from macroscopic  
311 quantities  $T$ ,  $\Omega$ ,  $F_N$  and  $h$ , the shear stress  $\tau$ , the normal stress  $\sigma$ , shear rate  $\dot{\gamma}$ , and the  
312 solid fraction  $\phi$  can be computed.

313

314 In the annular plate-cup shear geometry, the driving torque is converted into shear stress using  
315 the equation:

$$316 \quad T = \int_{R_i}^{R_o} 2\pi \cdot \tau \cdot r^2 dr \quad (4)$$

317 where  $\tau$  is the shear stress, and  $R_i$  and  $R_o$  are inner and outer radii of the annular trough.

318 If one neglects the radial velocity gradient (Clever et al. 2000; Coste 2004) into the annular  
319 trough, the shear stress is quasi-independent of the radial position  $r$  and thus, integrating Eq.  
320 (4) yields the shear stress as:

$$321 \quad \tau = 3T / 2\pi(R_o^3 - R_i^3) \quad (5)$$

322 Eq. (5) holds because the lateral contribution of wall frictions on the stress distribution within  
323 the granular media can be neglected. Indeed, for  $h = 30d$ , this relative contribution can be  
324 estimated to be of the order of  $\mu_w / \mu$  and we will see below that  $\mu_w / \mu \ll 1$ .

325

326 The normal stress can be also calculated from the normal force as follow:

$$327 \quad \sigma = F_N / \pi(R_o^2 - R_i^2) \quad (6)$$

328 Notice that for  $h = 10d$ , the imposed normal stress is larger than the hydrostatic pressure  
329  $\rho gh$  once  $F_N$  is larger than  $0.25N$ , meaning that gravity may be neglected for the range of  
330 imposed normal forces.

331

332 Besides, assuming that the velocity gradient is approximately uniform over the depth and  
 333 width of the annular trough and a no-slip condition exists at the rough upper and lower  
 334 shearing walls, one can estimate the mean shear rate as:

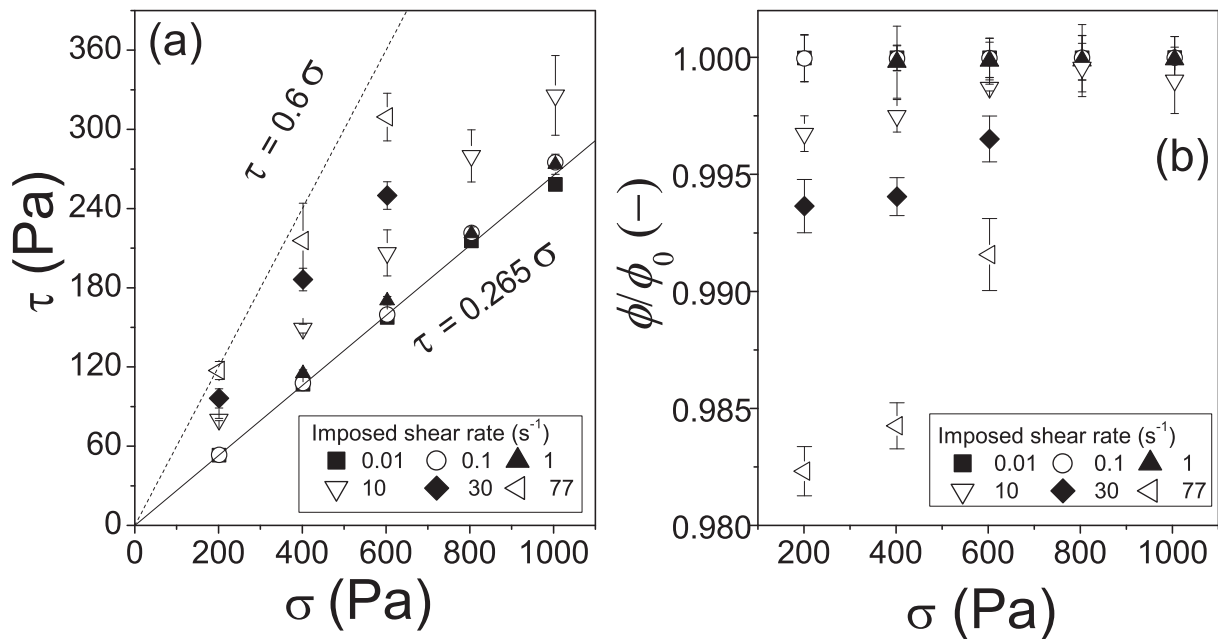
$$335 \quad \dot{\gamma} = \Omega(R_o + R_i)/2h \quad (7)$$

336 And the mean shear strain is given by:

$$337 \quad \gamma = \theta(R_o + R_i)/2h \quad (8)$$

338 where  $\theta$  is the angular displacement.

339 With this analysis, one can plot the shear stress in the steady state as a function of the normal  
 340 stress as in Figure 4a. The first observation is that a linear relationship between the shear and  
 341 normal stresses is seen for all imposed shear rates, with a slope that increases from 0.265 to  
 342 0.6 with increasing the shear rate. If an internal friction coefficient  $\mu$  is defined as the ratio  
 343 between shear and normal stresses, we evidence here that  $\mu$  is rate dependent: it increases  
 344 with  $\dot{\gamma}$ .



345  
 346 Figure 4: Plot of the shear stress (a) and of the solid fraction rescaled by its initial value  
 347 before shearing (b) as a function of the normal stress. The stress and the gap are measured in  
 348 the steady state, for different imposed shear rate. The error bars come from three experiment  
 349 runs.

350  
 351 The second observation is that, for all imposed shear rates, the steady value of the solid  
 352 fraction decreases when one decreases the normal stress (Figure 4b). Indeed, since the grains

353 cannot escape from the cell, one can measure unambiguously the solid fraction from the gap  
 354 variation as:

$$355 \quad \phi = m / \pi \rho h (R_o^2 - R_i^2) \quad (9)$$

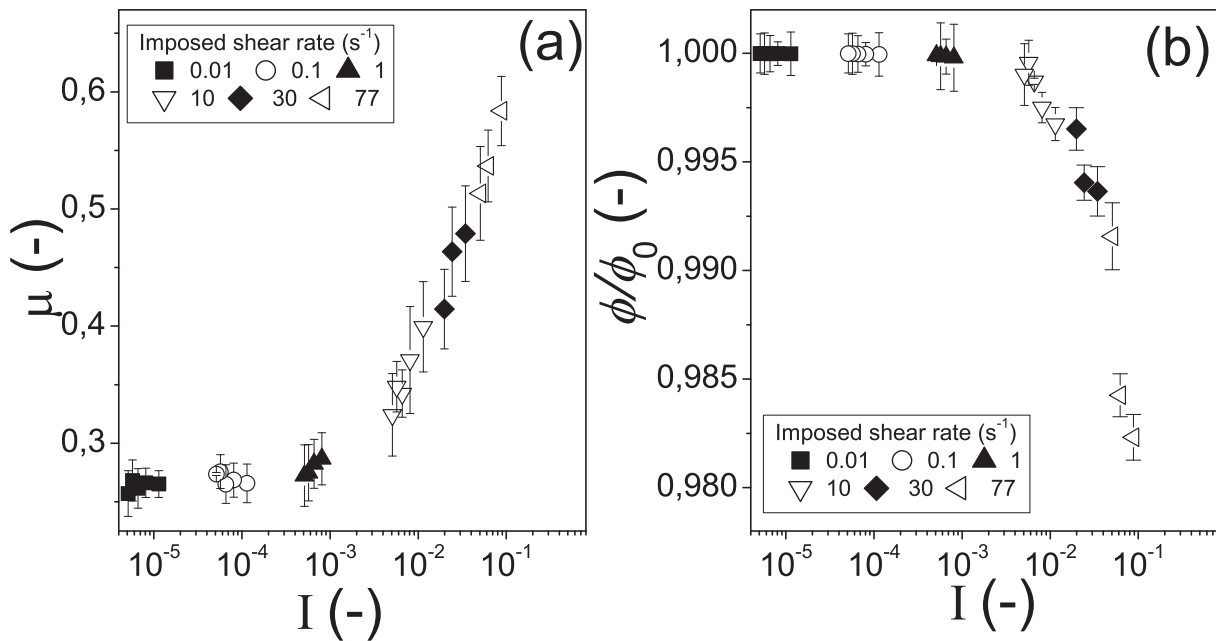
356 in which  $m$  represents the mass of grains. Thus  $h_o/h = \phi/\phi_0$  will simply reflect the impact of  
 357 shear and confinement on dilatancy.

358 In order to analyse the results in term of  $\mu(I)$ -rheology, one has to define an inertial number  
 359 such as:

$$360 \quad I = \dot{\gamma} d / \sqrt{\sigma / \rho} \quad (10)$$

361 in which  $\sigma$  is the normal stress in the steady state regime. It varies between  $10^{-7}$  and 0.1 in  
 362 the range of applied normal force and shear rate. This corresponds to the usual range of quasi-  
 363 static to dense flow regimes. It should be noted that our annular shear geometry does not  
 364 allow higher values of  $I$  to be studied.

365



366

367 Figure 5: Constitutive law for different sets of mean shear rates and imposed normal forces  
 368 (a) ‘friction law’ i.e. effective internal friction coefficient as a function of inertial number; (b)  
 369 ‘dynamic dilatancy law’ i.e. solid fraction as a function of inertial number. The error bars  
 370 come from three experiment runs.

371

372 Figure 5a shows how  $\mu$  vary throughout the flow regimes since  $I$  characterizes the local  
 373 ‘‘rapidity’’ of the flow. All the data obtained for different sets of shear rate and normal force  
 374 collapse on a single curve  $\mu = \tau/\sigma$  vs.  $I$ . For low inertial number, the internal friction

375 coefficient tends to a finite value  $\mu_s \approx 0.265$  and increases with increasing  $I$ . At the same  
 376 time, the solid fraction variation  $\phi/\phi_0$  with the inertial number  $I$  is shown in Figure 5b. Once  
 377 again, all the data collapse on a single curve. At low  $I$ ,  $\phi/\phi_0$  is quasi-constant: this is the  
 378 quasi-static regime. When  $I$  increases, the inertia starts influencing the flow and the system  
 379 becomes rate dependent: the ratio  $\phi/\phi_0$  decreases; this regime corresponds to the dense flow  
 380 in which the granular material dilates.

381  
 382 Moreover, in order to check the robustness of our results, we have varied the initial size of the  
 383 gap. Here, with our annular shear geometry, the same experiments discussed above are made  
 384 with different gap sizes from  $6d$  to  $22d$  and different sets of imposed shear rate and normal  
 385 force (Table 1).

Shear rate ( $s^{-1}$ )	Normal force $F_N$ (N)	Gap ( $h_0/d$ )
0.01	1-2-3-4-5	6-8-15
0.1	1-2-3-4-5	6-8-10
1	1-2-3-4-5	6-10-15
10	1-2-3	6-15
30	1-2-3	6-15-22
77	1-2-3	6-15-22

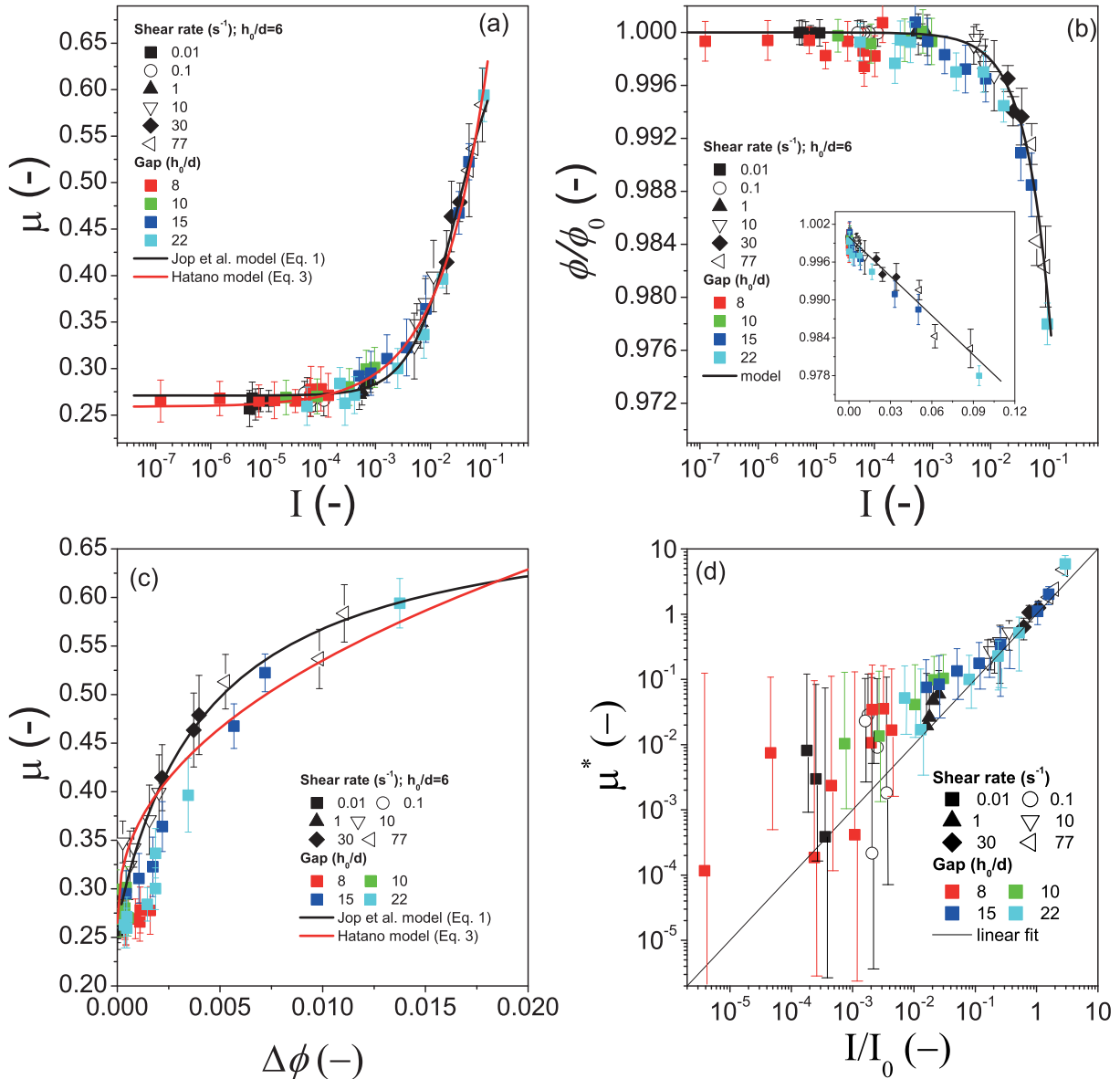
386 Table 1: Values of the imposed shear rate and normal force for each gap size.

387  
 388 It is shown in Figure 6 that changing the gap does not significantly affect these results. This  
 389 suggests a total absence of shear localization at high inertial number. However, at small  
 390 inertial number, the resolution of our measurements is not sufficient to dismiss the possibility  
 391 that shear localization arises. It was indeed shown that in confined annular flow at small shear  
 392 velocities and high confining pressures – small  $I$  –, the shear may be not homogeneous and  
 393 solid and fluid phases coexist (Aharonov & Sparks 2002; Jalali et al. 2002).

394  
 395 We now compare these experimental results with existing models such as those of Jop et al.  
 396 Eq. (1) and Hatano Eq. (3) on dry granular flows in terms of quasi-static and dense flow  
 397 behaviours. Concerning the ‘friction law’, our experimental data include points in range of  $I$   
 398 from  $10^{-7}$  to 0.1 which covers quasi-static and dense flow regimes. Our measurements then  
 399 show that, in this range of  $I$ , both models can describe our data. Using a classical least  
 400 squares method, the fit of the data gives:  $I_0 \approx 0.032 \pm 0.003$ ,  $\mu_s \approx 0.271 \pm 0.002$  and



401  $\mu_2 \approx 0.68 \pm 0.02$  for the ‘*Jop et al. model*’;  $\mu_s \approx 0.259 \pm 0.002$ ,  $a \approx 1.12 \pm 0.05$  and  
 402  $n \approx 0.49 \pm 0.02$  for the ‘*Hatano model*’. In Figure 6b, we show the ‘*dynamic dilatancy law*’,  
 403 i.e., the variation of the solid fraction  $\phi$  as a function of the inertial number  $I$ . We observe  
 404 that  $\phi$  decreases linearly with  $I$ , starting from a maximum value  $\phi_c$  in the quasi-static regime  
 405 where the granular material is very dense, close to the maximum solid fraction. The ‘*dynamic*  
 406 *dilatancy law*’ is thus given as:  $\phi/\phi_c = 1 - (1 - \phi_m/\phi_c)I$  with  $\phi_c \approx \phi_0 \approx 0.625$  and  
 407  $\phi_m \approx 0.495 \pm 0.002$  in agreement with (Pouliquen et al. 2006; Jop et al. 2005).



408  
 409 Figure 6: Constitutive law for different sets of mean shear rates and imposed normal forces,  
 410 and different gap sizes (Table 1): (a) ‘*friction law*’ i.e. internal friction coefficient as a  
 411 function of inertial number; (b) ‘*dynamic dilatancy law*’ i.e. solid fraction as a function of  
 412 inertial number; inset: the same data in linear scale. The solid line is  $\phi/\phi_c = 1 - (1 - \phi_m/\phi_c)I$

413 with  $\phi_c \approx \phi_0 \approx 0.625$  and  $\phi_m \approx 0.495$ ; (c) Internal friction coefficient vs. the reduced solid  
 414 fraction ( $\Delta\phi = \phi_c - \phi$ ); (d) Reduced internal friction coefficient as a function of the reduced  
 415 inertial number. The line is  $\mu^* = I/I_0$ . For each gap, the imposed shear rate varies from 0.01  
 416 to  $77 \text{ s}^{-1}$  depending of the imposed normal force in order to obtain either a low  $I$  (small  $\dot{\gamma}$   
 417 and/or large  $F_N$ ) or a high  $I$  (large  $\dot{\gamma}$  and/or small  $F_N$ ). The error bars come from three  
 418 experiment runs.

419

420 Combining the ‘*dynamic dilatancy*’ and the ‘*friction*’ laws, these data show that the internal  
 421 friction coefficient  $\mu$  strongly depends on the solid fraction: it decreases towards  $\mu_s$  when  $\phi$   
 422 tends to the maximum solid fraction (as shown on Figure 6c in which  $\Delta\phi = \phi_0 - \phi$  is the  
 423 reduced solid fraction). Moreover, following Staron and co-workers (Staron et al. 2010), we  
 424 defined a reduced internal friction coefficient  $\mu^*$  as:

$$425 \quad \mu^* = (\mu - \mu_s)/(\mu_2 - \mu) \quad (11)$$

426 We plot in the main panel of Figure 6d the resulting  $\mu^*$  vs.  $I/I_0$  data points. It holds  
 427 remarkably well with a prefactor of unity. Satisfying the ‘*Jop et al. model*’ implies indeed that  
 428  $\mu^* = I/I_0$  which is almost the case for our data except for small values of  $I$  ( $I < I_0 = 0.03$ )  
 429 wherein deviations seem to take place. The relationship between  $\mu^*$  and the reduced inertial  
 430 number is not clear. These deviations, observed in the quasi-static regime, were also  
 431 mentioned in recent studies which indicate that this rheology (the ‘*Jop et al. model*’) may be  
 432 not sufficient to describe the complex phenomena occurring at the flow threshold such as  
 433 intermittent flows (Mills et al. 2008), and is maybe strictly valid only for relatively large  
 434 inertial numbers (e.g.,  $I > 0.02$  as noted by Staron et al. 2010 and  $I > 0.005$  by Gaume et al.  
 435 2011). The reason for that is not clear yet but one possible explanation is shear localization  
 436 that arises most often in confined annular flow at small imposed shear and high pressure  
 437 (small inertial number  $I$ ) (Aharonov & Sparks 2002; Jalali et al. 2002; Koval 2009). Such  
 438 behavior of granular materials has not yet been fully understood and no consistent and general  
 439 formalism can predict it successfully (Kamrin 2012). In contrast to discrete numerical  
 440 simulations (Wang et al. 2012) and theoretical studies (Jenkins & Richman 1985; Richman &  
 441 Chou 1988; Jenkins 1992), the study of shear localization structure with experimental  
 442 methods is rather difficult. The visualization of the granular interface is usually limited to the  
 443 free surface or bottom layers (Fenistein and van Hecke 2003). Recently, MRI has been used

444 to study the granular rheology (velocity and solid fraction profiles) inside the granular system  
445 (Moucheront et al. 2010); this tool may thus be a great help in understanding the behaviour at  
446 low  $I$ . A change in the roughness of a boundary bottom might be used to modify the flow  
447 properties such as the wall slip velocity (Shojaee et al. 2012).

448

#### 449 **IV. Conclusion**

450 We have developed a rheometrical method in order to study dense granular flows with a  
451 rheometer under imposed confining normal stress and applied shear rate. From the steady  
452 state measurement of the torque and the gap, the internal friction coefficient, the solid fraction  
453 and the inertial number  $I$  are measured. For low  $I$ , the flow goes to the quasi-static limit and  
454 the internal friction coefficient and the solid fraction profiles are independent of  $I$ . Upon  
455 increasing  $I$ , dilation occurs and the solid fraction decreases linearly when  $I$  increases while  
456 the friction coefficient increases. The observed variations are in good agreement with  
457 previous observations of the literature. As a consequence, we bring evidence that rheometric  
458 measurements can be relevant to describe dry granular flows. However, additional  
459 experimental work should be carried out in order to measure the dependence of the boundary  
460 layer constitutive law on the state of the bulk material, so as to be able to describe properly  
461 the rheology when approaching the quasi-static limit.

462

#### 463 **Acknowledgments**

464 The authors thank P. Mills for useful discussions, a critical reading of the manuscript and  
465 many useful remarks.

466

#### 467 **References**

- 468 E. Aharonov & D. Sparks, *Shear profiles and localization in simulations of granular*  
469 *materials*, Physical Review E, 65:051302, 2002.
- 470 B. Andreotti, Y. Forterre and O. Pouliquen, *Granular Media: Between Fluid and Solid*,  
471 Cambridge University Press, 2013.
- 472 C. Ancey, P. Coussot, P. Evesque, *A theoretical framework for granular suspensions in a*  
473 *steady simple shear flow*, J. Rheol. 43 (6), 1673-1699, 1999.
- 474 I. S. Aranson, L. S. Tsimring, F. Malloggi, and E. Clement, *Nonlocal rheological properties*  
475 *of granular flows near a jamming limit*, Phys. Rev. E 78, 031303, 2008.

476 E. Azéma and F. Radjai, *Internal Structure of Inertial Granular Flows*, Phys. Rev. Lett. 112,  
477 078001, 2014.

478 R. A. Bagnold, *Experiments on a gravity free dispersion of large solid spheres in a newtonian*  
479 *fluid under shear*, Proc. Roy. Soc. London Ser. A, 225, 1954.

480 O. Baran and L. Kondic, *On velocity profiles and stresses in sheared and vibrated granular*  
481 *systems under variable gravity*, Phys. Fluids 18, 121509, 2006.

482 M. Becker and H. Lippmann, *Plane plastic flow of granular model material. Experimental*  
483 *setup and results*, Archiv of Mechanics, 29(6):829-846, 1977.

484 F. Boyer, E. Guazzelli, O. Pouliquen, *Unifying suspension and granular rheology*, Phys. Rev.  
485 Lett. 107, 188301, 2011.

486 J.-F. Camenen, Y. Descantes and P. Richard, *Effect of confinement on dense packings of rigid*  
487 *frictionless spheres and polyhedral*, Phys. Rev. E, 86, 061317, 2012.

488 J.F. Carr and D.M. Walker, *An annular shear cell for granular materials*, Powder Tech 1(6):  
489 369-373, 1968.

490 S. Chialvo, J. Sun, and S. Sundaresan, *Bridging the rheology of granular flows in three*  
491 *regimes*, Phys. Rev. E 85, 021305, 2012.

492 J.A.S. Cleaver, R.M. Nedderman and R.B. Thorpe, *Accounting for granular material dilation*  
493 *during the operation of an annular shear cell*, Adv. Powder Tech. 11, 4, 385-399, 2000.

494 C. Coste, *Shearing of a confined granular layer: Tangential stress and dilatancy*, Phys. Rev.  
495 E, 70, 051302, 2004.

496 F. da Cruz, S. Emam, M. Prochnow, J. Roux, and F. Chevoir, *Rheophysics of dense granular*  
497 *materials: Discrete simulation of plane shear flows*, Phys. Rev. E., 72:021309, 2005.

498 J. Duran, *Sands, powders and grains*, Springer-Verlag, New-York, 2000.

499 A. N. Edwards & J. M. N. T. Gray, *Erosion-deposition waves in shallow granular free-*  
500 *surface flows*, J. Fluid Mech., vol. 762, pp. 35-67, 2015.

501 D. Fenistein and M. van Hecke, *Wide shear zones in granular bulk flow*. Nature, 425:256,  
502 2003.

503 D. Fenistein, J.W. van de Meent, and M. van Hecke, *Universal and wide shear zones in*  
504 *granular bulk flow*, Phys. Rev. Lett. 92, 094301, 2004.

505 Y. Forterre and O. Pouliquen, *Flow of dense granular media*, Annual Reviews of Fluid  
506 Mechanics 40, 1-24, 2008.

507 GDR Midi. *On dense granular flows*. Euro. Phys. Journ. E., 14:341-365, 2004.

508 J. Gaume, G. Chambon, and M. Naaim, *Quasistatic to inertial transition in granular*  
509 *materials and the role of fluctuations*, Phys. Rev. E 84, 051304, 2011.

510 I. Goldhirsch, *Rapid granular flows*, Annual Reviews of Fluid Mechanics 35, 267-293, 2003.  
511 J. M. N. T. Gray & A. N. Edwards, *A depth-averaged  $\mu(I)$  – rheology for shallow granular*  
512 *free-surface flows*, J. Fluid Mech., vol. 755, pp. 503-534, 2014.  
513 T. Hatano, *Power-law friction in closely packed granular materials*, Phys. Rev. E, 75, 060301  
514 (R), 2007  
515 I. Iordanoff and M. M. Khonsari, *Granular lubrication: toward an understanding between*  
516 *kinetic and fluid regime*, ASME J. Tribol., 126:137–145, 2004.  
517 P. Jalali, W. Polashenski Jr., T. Tynjälä, and P. Zamankhan, *Particle interactions in a dense*  
518 *monosized granular flow*, Physica D, 162:188-207, 2002.  
519 A.W. Jenike, *Storage and flow of solids*, Bulletin No. 123, Utah Engineering Station, Salt  
520 Lake City, UT., 1964  
521 J. T. Jenkins and S. B. Savage, *A theory for the rapid flow of identical smooth nearly elastic*  
522 *spherical particles*, J. Fluid Mech. 130, 187, 1983.  
523 J. T. Jenkins and M. W. Richman, *Kinetic theory for plane flows of a dense gas of identical,*  
524 *rough, inelastic, circular disks*, Physics of Fluids, 28(12):3485, 1985.  
525 J. T. Jenkins, *Boundary conditions for rapid granular flows: Flat, frictional walls*. J. Appl.  
526 Mech., 59:120, 1992.  
527 P. Jop, Y. Forterre, and O. Pouliquen, *Crucial role of sidewalls in granular surface flows:*  
528 *consequences for the rheology*, J. Fluid Mech. 541, 167, 2005.  
529 P. Jop, Y. Forterre and O. Pouliquen, *A constitutive law for dense granular flows*, Nature  
530 441,727, 2006.  
531 K. Kamrin and G. Koval, *Nonlocal Constitutive Relation for Steady Granular Flow*, Phys.  
532 Rev. Lett. 108, 178301, 2012.  
533 G. Koval, J.-N. Roux, A. Corfdir, and F. Chevoir, *Annular shear of cohesionless granular*  
534 *materials: From the inertial to quasistatic regime*, Physical Review E, 79(2):021306,  
535 2009.  
536 G. Lois, A. Lemaitre, and J. M. Carlson, *Numerical tests of constitutive laws for dense*  
537 *granular flows*, Phys. Rev. E., 72, 051303, 2005.  
538 S. Luding, *The effect of friction on wide shear bands*, Part. Sci. Technol., 26-33, 2008.  
539 C.W. Macosko, *Rheology: Principles, Measurements and Applications*; Wiley VCH: New  
540 York, 1994.  
541 P. Mills, P. Rognon and F. Chevoir, *Rheology and structure of granular materials near the*  
542 *jamming transition*, Euro. Phys. Lett., 81, 64005, 2008.

543 P. Moucheron, F. Bertrand, G. Koval, L. Tocquer, S. Rodts, J.-N. Roux, A. Corfdir, and F.  
544 Chevoir, *MRI investigation of granular interface rheology using a new cylinder shear*  
545 *apparatus*, Magnetic Resonance Imaging, 28(6):910-918, 2010.

546 R.M. Nedderman, *Statics and kinematics of granular materials*. Cambridge University Press,  
547 Cambridge, 1992.

548 G. Ovarlez, C. Fond and E. Clément, *Overshoot effect in the Janssen granular column: a*  
549 *crucial test for granular mechanics*, Phys. Rev. E 67, 060302(R), 2003.

550 P-E. Peyneau and J-N. Roux, *Frictionless bead packs have macroscopic friction, but no*  
551 *dilatancy*, Phys. Rev. E 78:011307, 2008

552 O. Pouliquen, C. Cassar, P. Jop, Y. Forterre and M. Nicolas, *Flow of dense granular material:*  
553 *towards simple constitutive laws*, J. Statist. Mech., 7, P07020, 2006.

554 O. Pouliquen and Y. Forterre, *Friction law for dense granular flows: application to the*  
555 *motion of a mass down a rough inclined plane*, J. Fluid Mech., 453, 133-151, 2002.

556 M. W. Richman and C. S. Chou, *Boundary effects on granular shear flows of smooth disks*,  
557 Journal of Applied Mathematics and Physics (ZAMP), 39(6):885-901, 1988.

558 J. -N. Roux and G. Combe, *Rhéologie quasi-statique et origines de la déformation*, Comptes  
559 Rendus Physique 3, 131, 2002.

560 A. de Ryck, R. Ansart and J. A. Dodds, *Granular flows down inclined channels with a strain-*  
561 *rate dependent friction coefficient, Part I: Non-cohesive materials*, Granular Matter 10,  
562 353, 2008.

563 S. B. Savage and M. Sayed, *Stresses developed by dry cohesionless granular materials*  
564 *sheared in an annular shear cell*, J. Fluid. Mech., 142, 391-430, 1984.

565 S. B. Savage & K. Hutter, *The motion of a finite mass of granular material down a rough*  
566 *incline*, J. Fluid Mech., 199, 177-215, 1989.

567 A. Schoefield and P. Wroth, *Critical State Soil Mechanics*, McGraw-Hill, 1968.

568 Z. Shojaee, J.-N. Roux, F. Chevoir, D. E. Wolf, *Shear flow of dense granular materials near*  
569 *smooth walls. I. Shear localization and constitutive laws in the boundary region*, Phys.  
570 Rev. E 86 (1), 011301, 2012.

571 D. Schulze, *Flowability and time consolidation measurements using a ring shear tester*.  
572 Powder Handl Proc. 8:221-226, 1996.

573 J. Schwedes, *Review on testers for measuring flow properties of bulk solids*, Granular Matter  
574 5, 1, 2003.

575 L.E. Silbert, J. W. Landry & G. S. Grest, *Granular flow down a rough inclined plane:*  
576 *transition between thin and thick piles*, Phys. Fluids 15, 1-10, 2003.

- 577 L. E. Silbert, D. Ertas, G. S. Grest, T. C. Halsey, D. Levine, and S. J. Plimpton, *Granular flow*  
578 *down an inclined plane: Bagnold scaling and rheology*, Phys. Rev. E., 64:051302,  
579 2001.
- 580 L. Staron, P.-Y. Lagrée, C. Josserand, and D. Lhuillier, *Flow and jamming of a two-*  
581 *dimensional granular bed: Toward a nonlocal rheology?* Phys. Fluids 22, 113303,  
582 2010.
- 583 S. Torquato, T. M. Truskett, and P. G. Debenedetti, *Is Random Close Packing of Spheres Well*  
584 *Defined?* Phys. Rev. Lett. 84, 2064, 2000.
- 585 A. Tripathi and D. V. Khakhar, *Rheology of binary granular mixtures in the dense flow*  
586 *regime*, Phys. Fluids 23, 113302, 2011.
- 587 X. Wang, H. P. Zhu, and A. B. Yu, *Flow properties of particles in a model annular shear*  
588 *cell*, Phys. Fluids 24, 053301, 2012.
- 589 C.P. Wroth, *Soil behaviour during shear – existence of critical void ratios*, Engineering 186,  
590 409, 1958.